International Journal for Housing Science and Its Applications
Publish August 10, 2025. Volume 46, Issue 4 Pages 2340-2352

https://doi.org/10.70517/ijhsa464199

Energy Consumption Optimization Analysis of Fixed-Blade Paddle Wheels with Different Blade Inclination Angles Based on Fluent

Guankai Wang[1], Yihao Cheng[1], Changjiang Long[1,*], Zexu Hu[1], Wenpeng Yan[1] and Chundan Lu[1]
[1] School of Engineering, Huazhong Agricultural University, Wuhan, Hubei, 430000, China
Corresponding authors: (e-mail: huanonggch@163.com).

Abstract With the increasing demand for aquatic weed management in small and medium-sized aquaculture enterprises, existing propulsion systems such as propeller-driven, water-jet propulsion, and adjustable-blade paddle wheel-based weed-cutting vessels face challenges of poor adaptability and high costs, making them unsuitable for small-scale aquaculture farmers. This study employs the ANSYS Fluent hydrodynamic simulation model to investigate the mechanical characteristics and **energy consumption efficiency of a cost-effective, highly adaptable fixed-blade paddle wheel weed-cutting vessel under static water conditions. By establishing a three-dimensional model of the hull and paddle wheel, combined with dynamic mesh technology and User-Defined Functions (UDFs), this research simulates the thrust of the paddle wheel, hull resistance, and flow field distribution under varying blade inclination angles while maintaining consistent blade numbers and rotational speeds. Theoretical analysis is conducted to evaluate energy consumption performance under fixed rotational speeds. The results demonstrate that blade inclination angle significantly impacts energy consumption efficiency under identical rotational speeds and blade configurations. This study aims to provide a theoretical foundation for the design optimization of fixed-blade paddle wheel weed-cutting vessels, validate the **efficiency and reliability** of CFD simulations in naval hydrodynamic analysis, and lay the groundwork for subsequent energy consumption studies and energy-saving solutions in complex aquatic environments.

Index Terms ANSYS Fluent, fixed-blade paddle wheel, mechanical simulation, energy consumption analysis

I. Introduction

According to “2024 China Aquaculture Industry Panorama,” small and medium-sized aquaculture enterprises account for more than 90% of the Chinese aquaculture industry, and small aquaculture farmers are the main component of these small and medium-sized enterprises [1]. During aquaculture operations, waterweed density is a critical parameter. Excessive waterweed proliferation not only disrupts aquatic ecosystems but also directly impacts aquaculture efficiency [2]. Therefore, effectively controlling waterweed density has become an urgent issue for the aquaculture industry. Currently, common waterweed management solutions on the market primarily include propeller-driven, jet-driven, and paddlewheel-driven systems [3]. Li Chuang pointed out that propeller-driven systems are easy to design but may experience reduced propulsion efficiency and increased maintenance costs due to aquatic plant entanglement in shallow water aquaculture environments [4]. Liu Chengjiang et al. noted that while jet-driven systems partially mitigate aquatic plant entanglement issues, they exhibit low propulsion efficiency, high energy consumption, and high maintenance costs [5]. These limitations make propeller-driven and jet-driven systems unsuitable for meeting the large-scale aquatic plant management needs of the aquaculture industry. In recent years, paddlewheel-propelled aquatic weed cutting boats have garnered significant attention due to their excellent adaptability in shallow and complex aquatic weed environments [6]. Specifically, Ren Dongliang et al. [7] utilized an eccentric mechanism to adjust the angle of the blades entering and exiting the water, aiming to achieve maximum thrust and minimum resistance. This design grants paddlewheel-propelled systems a distinct advantage in large-scale and complex aquatic environments. However, the high manufacturing costs, substantial post-installation maintenance expenses, and requirements for operator expertise associated with movable-blade paddle wheels [8] have limited their widespread adoption among small-scale aquaculture farmers. In contrast, fixed-blade paddle wheels, as a structurally simple and cost-effective propulsion solution, reduce complexity and maintenance costs through their fixed-blade design [9], making them more suitable for small and medium-sized aquaculture enterprises and small-scale farmers. However, most current fixed-blade propeller designs feature a structure with six blades and no blade angle, resulting in low propulsion efficiency, high energy consumption, and an inability to

meet the demands of efficient operation in complex water environments. Therefore, the design and optimization of fixed-blade propellers still face numerous challenges.

Computational fluid dynamics (CFD) simulation technology provides an efficient and cost-effective research tool for ship design and optimization [10]. Using tools such as ANSYS Fluent, the interaction between paddle wheels and fluids can be accurately simulated to analyze thrust, drag, and flow field distribution patterns. In recent years, domestic and international scholars have conducted preliminary explorations into the performance optimization of fixed-pitch paddle wheels. For example, Fan Jinling [11] and others used ANSYS simulation to analyze the stress distribution of fixed-pitch paddle wheel blades; some scholars, such as Shao Lei and Han Qingsong, conducted dynamic analyses of fixed-pitch paddle wheels based on Pro/E modeling [12], [13]; Yang Jinglei [14] and others studied the propulsion performance of fixed-paddle paddle wheels with different numbers of blades. Developed countries have explored the greening of river machinery earlier. For example, the Netherlands has adopted hydrogen fuel cell mowing boats to achieve zero emissions [15], but Seddiek [16]'s research indicates that the cost is high, with a single boat costing over 200,000 USD, making it difficult to promote; ERIK et al. introduced an intelligent grass-cutting boat that reduces energy consumption through path optimization using AI algorithms [17], but it still relies on traditional propulsion systems. However, there are currently few CFD studies on fixed-paddle paddlewheel grass-cutting boats, and existing research lacks in-depth investigation into the hydrodynamic characteristics of fixed-paddle paddlewheels in complex aquatic plant-filled water conditions, particularly the mechanisms by which deviation angles affect propulsion efficiency and energy consumption have not been fully elucidated. Therefore, systematic research and optimization are still needed to investigate the hydrodynamic characteristics and energy efficiency of fixed-paddle paddle wheels in complex aquatic plant environments.

This paper uses the ANSYS Fluent simulation platform in combination with the design parameters of fixed-paddle paddle wheels to study their hydrodynamic characteristics and energy efficiency in static water conditions. By establishing three-dimensional models with different numbers of blades and deflection angles and analyzing the thrust of the fixed-paddle propeller, hull resistance, and flow field distribution patterns under the same speed conditions, this study provides an initial theoretical exploration of energy efficiency and its influencing factors. The research results aim to provide a theoretical basis for the design optimization of fixed-paddle propeller weed-cutting boats and lay the foundation for subsequent energy consumption analysis and energy-saving scheme design under complex water conditions.

II. Numerical simulation methods

II. A.Introduction to fixed paddle wheels

A fixed-pitch paddle wheel is a traditional propulsion device whose blades (paddles) are fixed to the hub and cannot be dynamically adjusted for angle of attack. It propels water by rotating as a whole to generate a reaction force. Its design is simple and reliable, but its efficiency is lower than that of modern variable-pitch propellers. Its important parameters are shown in Table 1:

Table 1: Key Parameters of Paddle Wheels

Parameters	Typical value	Impact
Number of blades	6 to 12 pieces	Impact on water flow and thrust
Angle between blade plane and rotation plane	0° to 30°	Impact on thrust and efficiency
Blade dimensions	1/8 to 1/5 of wheel diameter	Impact on lift
Rotational speed	Set as needed	Impact on speed
Wheel diameter	Set according to draft depth	Impact on torque
Blade cross-sectional shape	Symmetrical airfoil or flat type	Impact on efficiency

This paper uses Fluent simulation and physical verification to study the effect of the angle between the blade plane and the rotation plane on efficiency, with the aim of optimizing the design of the fixed-pitch propeller angle.

II. B.Simulation Model Construction and Simplification

To balance computational efficiency and simulation accuracy, a simplified three-dimensional model of the hull and propeller was created using SolidWorks software. The simulation model of the hull was constructed based on actual dimensions, retaining key geometric features such as the size and installation position of the propeller, the position and shape of the cutting mechanism, while omitting non-critical details such as bolt holes and weld structures to reduce simulation complexity [18], as shown in Figures 1 and 2. For different blade deflection angles: 0°, 5°, 10°, 17.5°, and 24°, corresponding propeller models were constructed, as shown in Figure 3. Taking the 5° deflection angle as an example, the geometric parameters of the blades were strictly matched to the design conditions. This

method reduces the computational load while ensuring the geometric accuracy of the core flow field region. It is worth noting that due to the model's axis (face) symmetry, only half of the computational domain needs to be calculated during simulation [19], as shown in Figure 4.

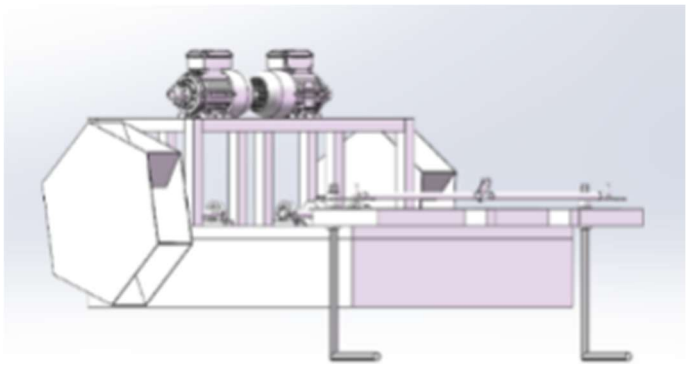

Figure 1: Physical modeling of an aquatic weed-cutting vessel

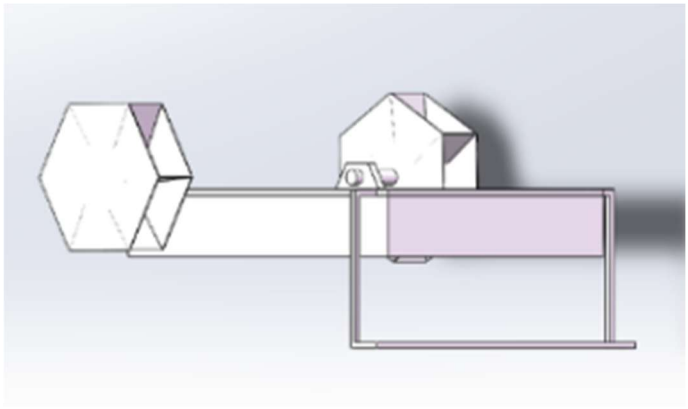

Figure 2: Simplified modeling of the cutting vessel

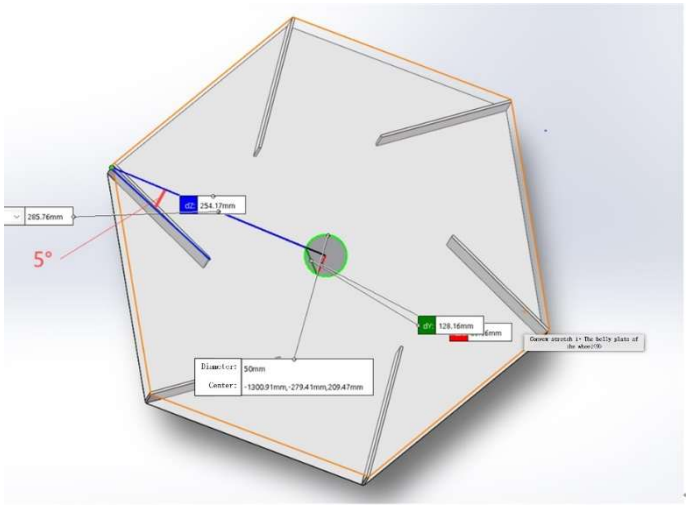

Figure3: 5° inclined paddle wheel modeling

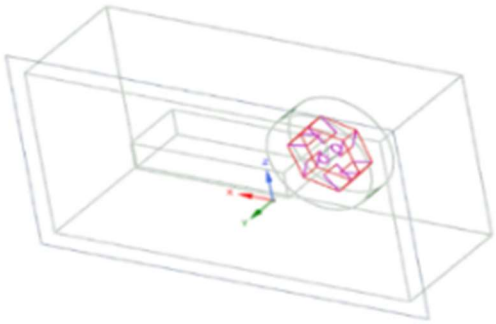

Figure 4: CFD domain for simulation

II. C.Numerical model

II. C. 1) Control equations and turbulence models

To accurately simulate the fluid dynamics behavior of a fixed-paddle wheel mowing boat, this study uses the Reynolds-averaged Navier-Stokes equations (RANS) as the governing equations (Liu Yingzhong [20]). The governing equation set includes the continuity equation, momentum equation, turbulent kinetic energy equation, and turbulent dissipation rate equation.

For incompressible fluids, the RANS equations can be expressed as:

$$\frac{\partial U_i}{\partial X_i} = 0 \text{ (Continuity equation)} \tag{1}$$

$$\rho\frac{\partial U_i}{\partial t} + \rho\frac{\partial}{\partial X_j}(U_i U_j + \overline{u_j' u_i'}) = -\frac{\partial P}{\partial x_i} + \frac{\partial}{\partial x_j}(2\mu s_{ji}) \text{ (Momentum equation)} \tag{2}$$

The k-ε turbulence model closed equation set is as follows [21]-[24]:

(1) Turbulent kinetic energy equation

$$\rho_1\frac{\partial k}{\partial t} + \rho_1\frac{\partial k}{\partial x_i}(ku_i) = \frac{\partial}{\partial x_j}(\alpha_k(\mu_1 + \mu_t)\frac{\partial k}{\partial x_j}) + G_k - \rho_1\varepsilon \tag{3}$$

(2) Turbulent dissipation rate equation (ε equation)

$$\rho_1\frac{\partial \varepsilon}{\partial t} + \rho_1\frac{\partial}{\partial x_i}(\varepsilon u_i) = \frac{\partial}{\partial x_j}(\alpha_\varepsilon(\mu_1 + \mu_t)\frac{\partial \varepsilon}{\partial x_j}) + C_{1\varepsilon}\frac{\varepsilon}{k}G_k - C_{2\varepsilon}\rho_1\frac{\varepsilon^2}{k} \tag{4}$$

Empirical constants in the closed equation system (standard k-ε model)

x_i, x_j are coordinate components, m; u_i is the velocity component, m/s; μ_1 is the dynamic viscosity of the fluid, $P_a \cdot s$; μ_t is the turbulent viscosity coefficient, $P_a \cdot s$; $C_{1\varepsilon}$, $C_{2\varepsilon}$ are empirical coefficients; ρ_1 is the fluid density, kg/m³; G_k is the term for the generation of turbulent kinetic energy k caused by the average velocity gradient; α_k, α_ε are the reciprocals of the turbulent Prandtl numbers associated with turbulent kinetic energy k and dissipation rate ε, respectively.

Based on empirical data, the values of the relevant parameters in the computational model are as follows: $C_{1\varepsilon}$ =1.42, $C_{2\varepsilon}$ =1.68

Fluid-structure interaction is implemented using dynamic mesh technology. The propeller rotation domain and the static water domain are coupled via a sliding interface to ensure the continuity of the momentum and mass conservation equations. The propeller blades are analyzed using a fluid-structure interaction approach. The finite element model in ANAYS can be used to relatively simply analyze the force conditions on fixed-pitch propeller blades.

II. C. 2) Combination of structured and unstructured grids

Regular regions: Structured hexahedral grids are used in geometrically regular regions such as the ship's symmetrical plane and propeller shaft. Their high orthogonality (orthogonality quality > 0.9) and low distortion (<0.3) significantly improve numerical stability [25].

Complex Regions: In regions with significant curvature changes, such as propeller blades and the ship-water interface, unstructured tetrahedral/polyhedral grids are used. Adaptive element sizes are employed to capture local flow details [26].

Hybrid domain partitioning: The propeller rotation domain uses a structured grid (size 25 mm), while the surrounding water domain uses an unstructured grid as shown in Figure 5 (size 50 mm). A sliding interface is used to achieve dynamic coupling between the rotating domain and the static domain.

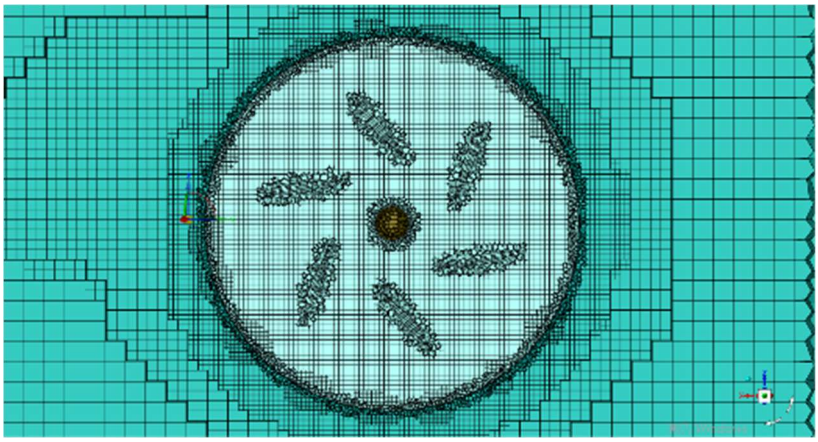

Figure 5: Rotating-static domain dynamic coupling

Global base grid: Based on the diameter of the paddle wheel (0.48 m), the initial grid size is set to 24 mm (1/20 of the diameter) to cover the entire calculation domain.

Surface of the paddle blade: Set up 10 layers of boundary layer grids, with a thickness of 0.1 mm for the first layer and a growth rate of 1.2, to ensure high-precision analysis of the flow near the wall [27].

Around the hull: An encrypted zone with a grid size of 8 mm, set at three times the length of the hull (1.2 m), accurately captures the flow characteristics around the hull.

Wake and vortex core region: Capture gradient flow characteristics such as blade tip vortices and waterweed region separation flows through local refinement with a grid size of 5 mm.

II. C. 3) Grid Quality Optimization and Validation

Aspect ratio: The aspect ratio of the global mesh is controlled within 5 to avoid numerical divergence caused by excessive stretching of the cells.

Distortion: The distortion of unstructured meshes is less than 0.4, and that of structured meshes is less than 0.2 to ensure computational stability.

Orthogonality quality: The global orthogonality quality is >0.1, and that of the core area (blade surface, hull) is >0.3.

Boundary layer transition: Prismatic layer grids are used to smoothly transition the boundary layer to the external region, avoiding pseudo-diffusion caused by sudden changes in size.

II. C. 4) Adaptive Mesh Refinement (AMR) and User-Defined Function (UDF) Development

Enable the AMR function in transient simulation to automatically refine high-resolution regions based on vortex flux thresholds, with a maximum refinement level of 2 [28]. This strategy reduces the total number of meshes by approximately 30% while ensuring accuracy in the wake region and vortex core region.

Write a UDF to implement mesh adaptive triggering [29], dynamically adjust the local mesh density based on pressure gradients, and monitor the output blade surface pressure distribution and hull resistance data in real time for subsequent analysis.

II. D.Boundary Conditions and Resistance Modeling

II. D. 1) Boundary Condition Settings [30]

Ship hull surface: Defined as a non-slip wall surface, standard wall functions are used to handle flow near the wall, satisfying the turbulence model requirements of y+ ≈ 30–100.

Propeller region: Dynamic mesh technology is used, with the rotational domain angular velocity set to 70 rpm (ω = 7.33 rad/s), and the rotational axis coinciding with the ship hull axis.

Calculation domain boundaries: The inlet is a velocity inlet under static water conditions with v = 0 m/s, the outlet is a pressure outlet (standard atmospheric pressure), and the lateral and bottom boundaries are symmetric.

II. D. 2) Simulation of aquatic plant resistance

The measured resistance data for aquatic plant cutting obtained using a force sensor ranges from 0 to 75 N. Using MATLAB, the resistance-time curve was fitted using cubic spline interpolation to obtain a smooth resistance function F(t). This resistance was then mapped to an additional volume force source term via a user-defined function (UDF) and uniformly applied to the area where the aquatic plants are distributed. This method ensures the dynamic characteristics of the resistance while avoiding the numerical instability of complex multiphase flow models.

II. E. Operating conditions design and evaluation indicators

II. E. 1) Operating conditions design

To investigate the influence of blade parameters on paddle wheel performance, five operating conditions were set according to Table 2, covering the variable of deviation angle, to analyze the effect of blade angle of attack on resistance distribution and energy efficiency.

The propeller speed was kept constant at 70 rpm. Based on Yang Jinglei's research results, it was concluded that six blades provide the best propulsion performance under normal conditions.

The waterweed resistance was uniformly distributed over the front section of the hull, covering an area of 1.2 m².

Table 2: Design of various operating conditions

Operating condition number	Operating conditions description
Operating condition 1	Blade deviation angle from center 0°
Operating condition 2	Blade deviation angle from center 5°
Operating condition 3	Blade deviation angle from center 10°
Operating condition 4	Blade deviation angle from center 17.5°
Operating condition 5	Blade deviation angle from center 24°

II. E. 2) Evaluation Indicators

Energy efficiency estimation is used as the evaluation index: the force curve diagram of the paddle wheel thrust is used to calculate the output power of the paddle wheel within one cycle, and the average value of the input power P1 of the paddle wheel is calculated over multiple cycles. Among them, $F(t)$ is the thrust on the paddle wheel, ω is the angular velocity, and r is the radius of the paddle wheel. The effective power P2 is calculated using the force curve diagram of the paddle wheel thrust and the force curve diagram of the resistance. The formula is as follows:

$$V = \omega \cdot r \tag{5}$$

$$\mathrm{P1} = 2V \times \int_0^T F(t)dt \tag{6}$$

$$\mathrm{P2}=2\times \int_0^T F(t)dt - \left| \int_0^T f(t) \right| dt \tag{7}$$

$$\eta = \frac{\mathrm{P2}}{\mathrm{P1}} \times 100\% \tag{8}$$

where $F(t)$ is the thrust exerted on the paddle wheel, $f(t)$ is the drag force exerted on the entire ship, P1 is the input power, P2 is the effective power, T is the period time, ω is the angular velocity, r is the radius of the paddle wheel, V is the linear velocity at the end of the paddle wheel, and η is the efficiency.

III. Numerical simulation results and analysis

III. A. Data Processing and Analysis

III. A. 1) Flow field data extraction

The distribution characteristics of the velocity field, pressure field, and streamlines under different operating conditions are extracted and displayed using cloud maps and vector diagrams (Figure 6).

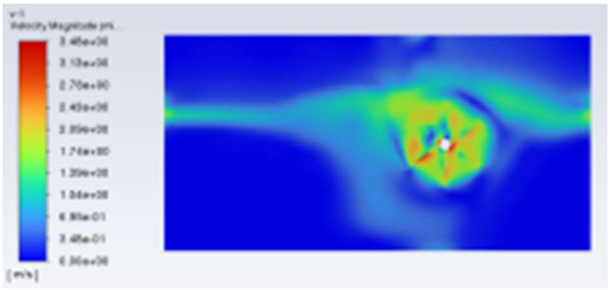

(a) 0°

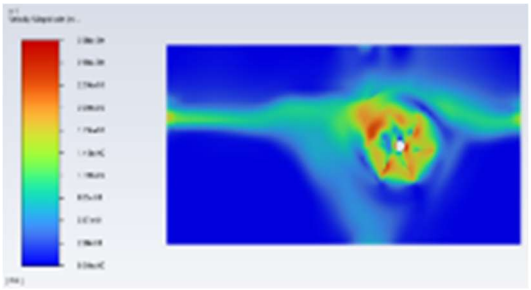

(b) 5°

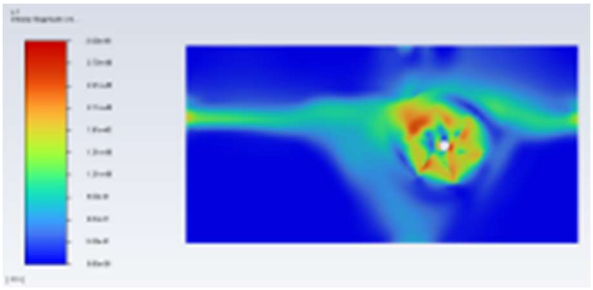

(c) 10°

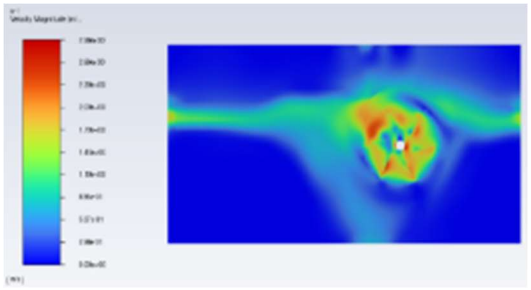

(d) 17.5°

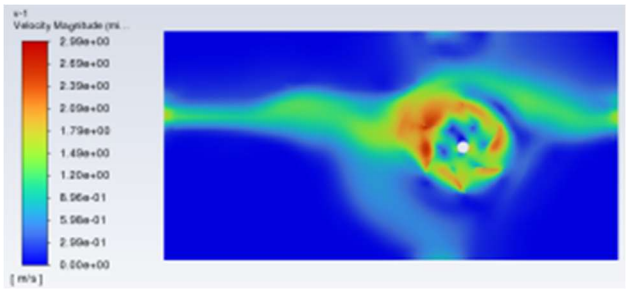

(e) 24°

Figure 6: Flow velocity contours for various working conditions

III. A. 2) Extraction of force data

The force curves for hull resistance and paddlewheel thrust under different operating conditions are extracted separately, as shown in Figures 7 and 8.

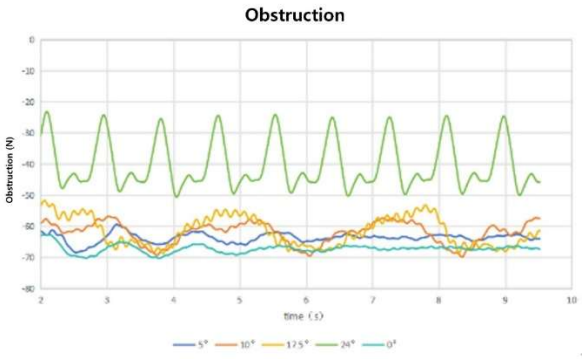

Figure 7: Resistance performance across various working conditions

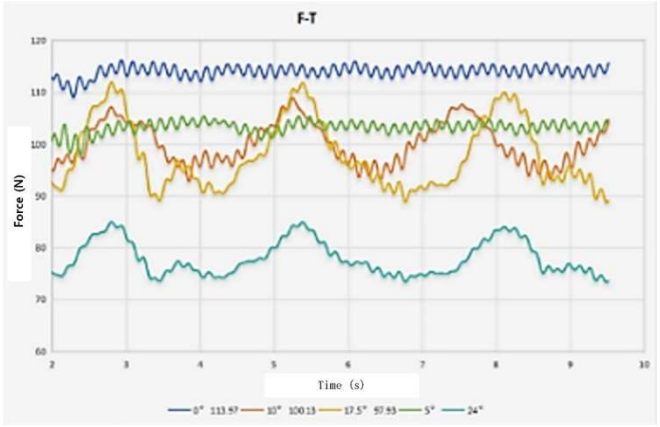

Figure 8: Thrust performance across various working conditions

III. B. Flow Field Characteristics Analysis

III. B. 1) Effect of blade deviation angle on flow field

Under the condition of a fixed number of six blades, as the angle of deviation from the center increases from 0° to 28°, the vortex structure generated by the propeller rotation gradually evolves from a symmetric distribution to an asymmetric one. According to the drag curve, a sudden drop in drag occurs at an angle of 24°, with a slight recovery at 28°. The following analysis focuses on the velocity contour plots and streamlines at the special case of a 24° deflection angle, as shown in Figures 9 and 10.

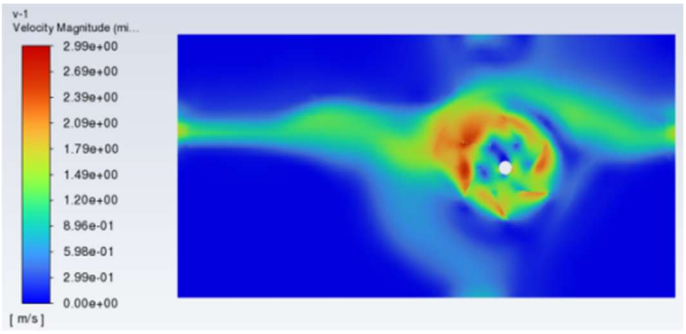

Figure 9: Flow Velocity Field Visualization for 24° Paddle Wheel Configuration

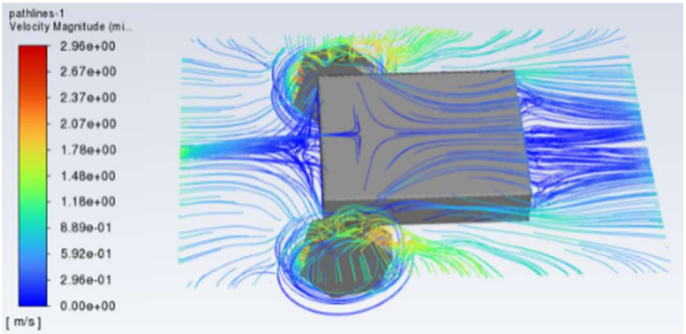

Figure 10: Flow Trace Diagram at 24° Inclination Angle

The velocity distribution can be determined from the figure: High-speed zone at the leading edge (2.96 m/s): The water flow accelerates at the leading edge of the blade, forming a local low-pressure zone and generating effective thrust. Low-speed zone at the trailing edge (0.89–1.48 m/s): Flow separation causes kinetic energy dissipation, but the velocity gradient is gentle, reducing turbulence losses.

Pressure distribution: The pressure difference between the low-pressure zone at the leading edge and the high-pressure zone at the trailing edge creates pressure difference drag, but the separated vortices may reduce net drag through energy redistribution.

Vortex structure: Large-scale separated vortices exist behind the blade, with lower pressure at the vortex core center, which may suppress the growth of pressure difference drag.

Analysis of key phenomena reveals that at an angle of attack of 24°, the leading edge velocity reaches 2.96 m/s, causing a local pressure drop (Bernoulli's principle), reducing the pressure difference between the front and rear of the blade, and thereby reducing pressure difference drag. The trailing edge separation vortex forms a stable structure, with part of its rotational kinetic energy converted into propulsive energy (similar to the vortex shedding mechanism in fish swimming), reducing energy dissipation. Flow separation reduces shear stress on the blade surface, decreasing the proportion of friction resistance. Combining the analysis with the figure, an increase in blade angle reduces the effective flow area, causing the lift component (thrust) to decrease gradually with increasing angle of attack. Although input power decreases significantly due to reduced thrust, net propulsion power decreases only slightly due to reduced resistance, resulting in an efficiency improvement to 74.3%. Comparison with other angle of attack conditions is shown in Table 3.

Table 3: Flow Field Comparison: 24° Case vs. Baseline Conditions

Angle (°)	Flow field characteristics	Experimental results
0°–17.5°	Laminar flow with no significant vortices	Linear decrease in thrust, steady increase in drag
24°	Large-scale separation vortices, high-speed zone at the leading edge	Decrease in thrust, significant decrease in drag

III. B. 2) Inhibitory effect of aquatic plant resistance on flow velocity

The flow velocity in the aquatic plant area is reduced to 0.2-0.4 m/s under all operating conditions. When the deviation angle is 0°, the pressure gradient in the aquatic plant area is minimal, indicating that when the blade cuts vertically into the aquatic plants, the concentration of resistance can be partially alleviated.

III. C. Force and Energy Consumption Analysis

III. C. 1) Effect of blade deviation angle on thrust and drag

Under conditions where the number of blades is fixed at 6, thrust decreases linearly as the deflection angle increases. At a deflection angle of 0°, thrust reaches a peak of 113.97 N, while at a deflection angle of 28°, thrust is only 68.273 N. Unlike thrust, drag increases slowly as the deflection angle increases from 0° to 17.5°. However, when the angle further increases to 24°, drag suddenly decreases to -40.748 N. At 28°, drag increases slightly but remains lower than that at angles between 0° and 17.5°.

III. C. 2) Efficiency Calculation

The thrust and drag obtained from the simulation were calculated using evaluation indicators to obtain Table 4.

Table 4: Performance Efficiency Analysis for Multiple Working Conditions

Angle (°)	Input power (W)	Effective power (W)	Efficiency (%)
0°	401.2	283.6	70.7%
5°	363.0	251.0	69.2%
10°	352.4	243.2	69.0%
17.5°	344.4	237.4	68.9%
24°	278.1	206.7	74.3%

Since the maximum value is obtained at an angle of 24°, increasing the operating angle to 28° reveals an average thrust of 68.273 N and a drag force of 46.682 N. Based on the above formula, theoretical analysis shows that the input power is 240.32 W. The effective power is 158.16 W. The efficiency is only 65.8%.

III. C. 3) Effect of blade deviation angle on efficiency

With the number of blades fixed at six, it is easy to see from the table and analysis that the efficiency does not change much between 0° and 17.5°, showing a slight downward trend overall. The efficiency increases significantly at an angle of 24°, but decreases at an angle of 28°. There must be an optimal working angle in the 24° range, which is estimated to be between 23° and 25°.

IV. Physical verification

The aim is to verify the accuracy of the Fluent-based CFD simulation model in predicting thrust, drag, and energy consumption of a fixed-paddle paddlewheel mower boat in still water conditions. In addition, the differences between

the experimental data and simulation results under the base operating condition of 0° blade angle and the simulated optimal operating condition of 24° blade angle are compared, and the sources of error are analyzed.

IV. A. Experimental Platform and Equipment

IV. A. 1) Test tank

Conducted at the Aquaculture Base of Huazhong Agricultural University, requiring a still water environment with a flat bottom and smooth side walls to reduce boundary interference.

Dimensions: Length × Width × Depth = 10 m × 3 m × 1.5 m.

IV. A. 2) Paddlewheel experimental prototype

Hull dimensions: Length × Width × Thickness = 1.2 m × 1 m × 0.2 m, consistent with the simulation model.

Propeller parameters: Six stainless steel propeller blades with offset angles of 0° and 24°, rotation speed of 70 rpm, and motor rated power of 750 W.

IV. A. 3) Measuring equipment

Force sensor: Installed at the connection between the paddle wheel shaft and the hull and at the bow, it collects real-time thrust and drag data (range 0–200 N, accuracy ±0.5% FS).

Tachometer: Monitors the actual speed of the paddle wheel (accuracy ±1 rpm).

Data acquisition system: Synchronously records force, speed, and flow velocity signals with a sampling frequency of ≥100 Hz.

IV. A. 4) Aquatic Plant Simulation Device

Flexible aquatic plant-like materials (such as nylon threads) are evenly distributed at the front of the hull (covering an area of 1.2 m² with a drag range of 0–75 N).

The drag of the aquatic plant-like materials is calibrated using a tensile meter to ensure consistency with the drag function loaded in the simulation UDF.

IV. B. Experimental Design and Parameter Settings

IV. B. 1) Effect of blade deviation angle on efficiency

Set two sets of deviation angles at 0° and 24°, respectively, with waterweed resistance distributed uniformly. The specific parameters of the experimental prototype are shown in Table 5.

Table 5: Detailed Parameters of the Experimental Prototype

Parameters	Numerical
Length*Width*Thickness	1.2m*1m*0.2m
Motor rated power	750W
Propeller speed	70rpm
Overall mass	120kg
Number of blades	6
Blade thickness	3mm
Number of propellers	2

IV. B. 2) Experimental procedure

Step 1: Calibrate the sensors and equipment to ensure that the data acquisition system is synchronized.

Step 2: Secure the hull in the center of the pool and start the motor at the set speed.

Step 3: After the system has stabilized (approximately 30 seconds), continuously collect thrust, drag, and flow velocity data for 5 minutes.

Step 4: Repeat the experiment three times and take the average value to eliminate random errors.

Step 5: Replace the paddle wheel and repeat steps 2 to 4.

IV. C. Comparison and analysis of experimental results and simulation results

Use MATLAB to plot comparison graphs of thrust-angle and drag-angle curves for experimental and simulation data, analyze trend consistency, and calculate their average values.

Using Figures 11 and 12, we obtain an average experimental thrust of 109.3 N and drag of 75.7 N at an angle of 0°, and an average experimental thrust of 66.1 N and drag of 41.2 N at an angle of 24°.

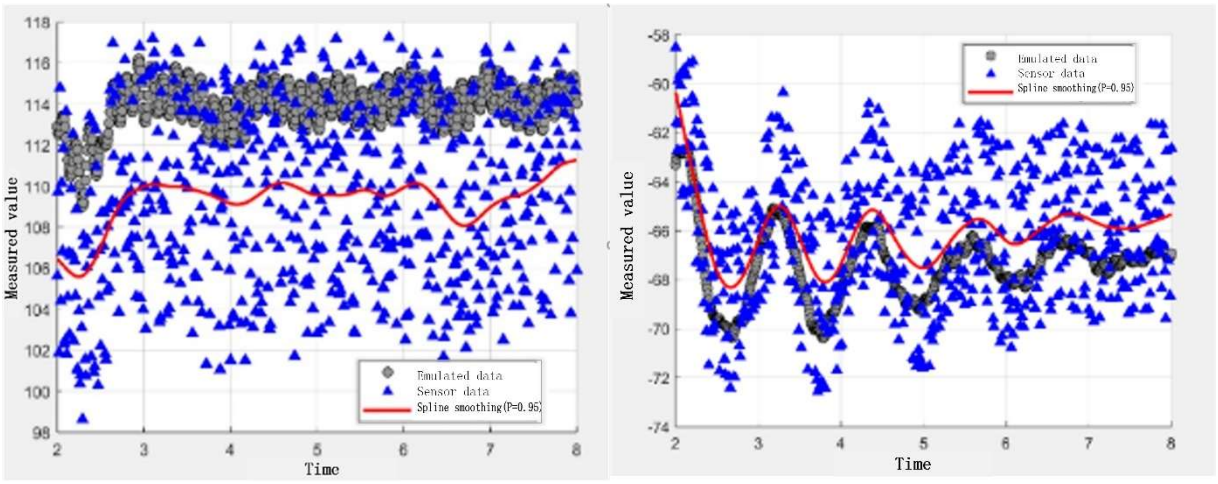

Figure 11: Thrust and Resistance at 0° Inclination Angle

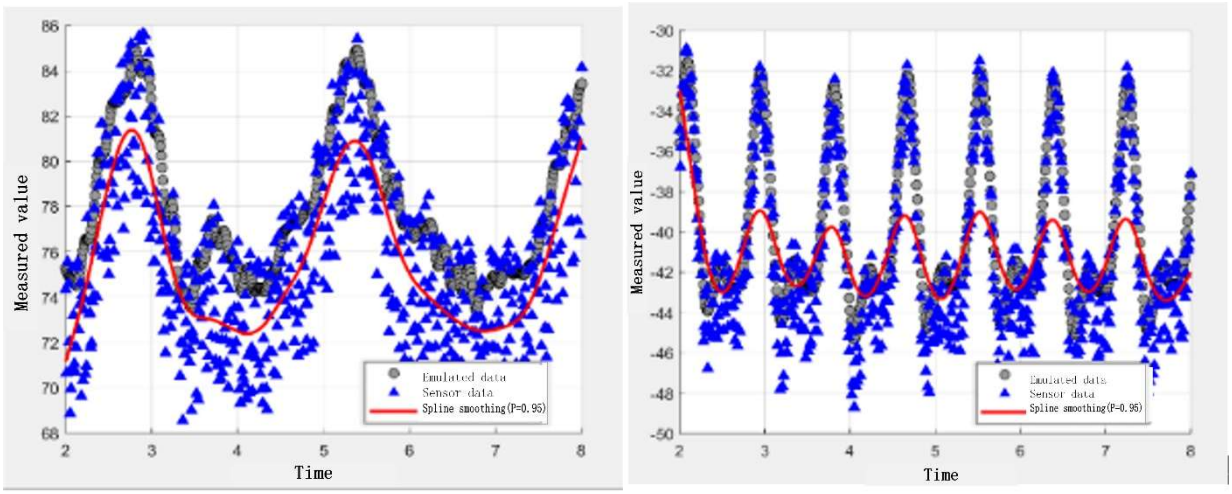

Figure 12: Thrust and Resistance at 24° Inclination Angle

Based on the above analysis, the efficiency calculation formula can be obtained as shown in Table 6.

Table 6: Performance Benchmarking: Experimental vs. Computational Efficiency

Offset angle (°)	Physical efficiency (%)	Simulation efficiency (%)	Error (%)
0°	X	70.7	1.3
24°	X	74.3	2.0

Main sources of error: actual flow field turbulence intensity, mechanical friction loss, and uneven distribution of aquatic plant resistance.

IV. D. Physical verification conclusions

Through comparative analysis of actual ship testing and simulation data, the reliability of the CFD model in predicting thrust, drag, and energy consumption under static water conditions was verified (average error less than or equal to X%). The experimental results support a 24° deviation angle as the optimal design parameter, providing empirical evidence for subsequent engineering applications.

V. Conclusions and Discussion

V. A. Conclusion

This study employs computational fluid dynamics (CFD) simulation technology, combined with moving mesh technology and user-defined functions (UDFs), to accurately quantify the impact of aquatic vegetation resistance

on the performance of paddle wheels during operation. Traditional research methods are often limited to static analysis, making it difficult to accurately reflect the dynamic effects of aquatic vegetation resistance on paddle wheel performance. The innovation of this study lies in using moving mesh technology to simulate the actual motion trajectories of paddle wheel blades and combining UDF to dynamically load the aquatic plant resistance model, thereby more accurately reflecting the operational state of paddle wheels in complex aquatic environments. This enhances the accuracy of simulation results and provides a reliable theoretical basis for the optimized design of fixed-pitch paddle wheels.

This study reveals the interaction patterns between blade deviation angle and blade number on paddle wheel thrust and resistance. Through extensive simulation experiments and data analysis, a significant coupling effect was found between blade deviation angle and blade number. When the blade number is fixed at 6 blades and the blade deviation angle is 24°, the paddle wheel achieves an optimal balance between thrust and resistance, significantly improving propulsion efficiency. This finding provides a clear direction for parameter optimization in paddle wheel design and has direct engineering application value.

V. B. Discussion

To further improve the propulsion efficiency of paddle wheels, more detailed optimization studies are needed within the blade deflection angle range of 23° to 25°. By combining numerical simulation and experimental methods, the thrust, drag, and energy consumption characteristics of paddle wheels at different angles are analyzed to determine a more accurate optimal angle range. Additionally, the coupled effects of blade shape and angle are considered to explore their influence on flow field distribution, providing more precise theoretical basis for paddle wheel design.

Current research primarily focuses on the performance analysis of paddle wheels under static water conditions. However, real-world aquatic environments are complex and dynamic, and factors such as waves and varying flow speeds significantly impact paddle wheel performance. Future research should incorporate dynamic operating conditions by establishing a wave-paddlewheel coupling model to analyze thrust fluctuations, structural stress distribution, and energy consumption characteristics of the paddlewheel under wave action. Additionally, the impact of flow velocity changes on paddlewheel propulsion efficiency should be considered, and adaptive optimization strategies for the paddlewheel under different flow velocity conditions should be explored.

To achieve efficient operation of paddle wheels in complex aquatic environments, it is necessary to develop intelligent control strategies based on aquatic plant density distribution. By integrating sensor and data analysis technologies, real-time monitoring of aquatic plant distribution and flow conditions can be achieved, enabling dynamic adjustment of paddle wheel speed to optimize energy efficiency. Additionally, by integrating navigation systems, autonomous path planning and obstacle avoidance functions can be realized, further enhancing the applicability and economic viability of paddle wheels in large-scale aquaculture facilities.

References

[1] Cai Zhihao. Forecasting 2024: “A Comprehensive Overview of China's Aquaculture Industry in 2024” [EB/OL]. (2024-11-15) [2025-4-18].
[2] Zhu Enhhe, Li Baoyan, Li Junli. Waterweed proliferation hazards and countermeasures in Erwangzhuang Reservoir [J]. Water Science and Engineering Technology, 2010, (05): 55-56.
[3] Lin Jianhui, Lu Sheng. Review of propulsion schemes for small LNG ships [J]. Ship and Ocean Engineering, 2012(3): 52-55, 61.
[4] Li Chuang, Li Zhi. Research on Propulsion Forms of Ship Propellers [J]. Ship Electrical Technology, 2016, 36(12): 68-73.
[5] Liu Chengjiang, Wang Yongsheng, Ding Jiangming. Review of Waterjet Propulsion Research [J]. Ship Engineering, 2006, 28(4): 49-52.
[6] Sun Bin. Trajectory Planning and Control of Surface Unmanned Vessels with Paddle Wheel Propulsion [D]. Jiangsu: Jiangsu University of Science and Technology, 2021.
[7] Ren Dongliang. Improved paddle wheel propeller: CN201420228016.3[P]. 2014-10-01.
[8] Shanghai Ocean University. A type of amphibious vehicle walking mechanism with paddle wheels: CN201620273669.2[P]. 2016-08-10.
[9] Huan Qing Huang. Research on Paddle Wheel Propulsion for Small Clean Boats in Inland Rivers [D]. Jiangsu: Jiangsu University of Science and Technology, 2013.
[10] Li Min. Analysis of wave-induced drag characteristics and hull form optimization design of high-speed vessels [J]. Ship Science and Technology, 2023, 45(4): 41-44.
[11] Fan Jinling, Wang Zhehe, Jiang Haiyong, et al. Fluid-structure interaction analysis of paddle wheels based on ANSYS [J]. Agricultural Machinery Research, 2013(4): 33-36.
[12] Shao Lei. Modal and dynamic analysis of propeller for aquatic weed harvester based on Pro/E [J]. Research and Application of Machinery, 2009, 22(6): 32-34.
[13] Han Qingsong, Shang Shiyou, Wang Zhiguo, et al. Modeling and simulation of a propeller device for a water grass harvester based on Pro/E [J]. Agricultural Mechanization Research, 2006(6): 95-97.
[14] Yang Jinglei, Deng Zhipeng, Hou Liang, et al. High-speed propeller performance with different numbers of blades [J]. Journal of Guangdong Ocean University, 2024, 44(3): 136-142.
[15] Netherlands Develops New Hydrogen Storage Technology for Fuel Cells [J]. New Materials Industry, 2011, (11): 88-89.
[16] S. I S, R. N A. Carbon footprint and cost analysis of renewable hydrogen-fuelled ships[J]. Ships and Offshore Structures, 2023, 18(7): 960-969.

[17] ERIK STENSRUD, PIERRE SAMES, ΦYVIND SMOGELI, et al. Artificial Intelligence in the maritime industry[C]//World Maritime Technology Conference 2018(WMTC18) Proceedings. 2018:1-16.
[18] Chen Huang, Lin Xiongping. Application of computational fluid dynamics in ship maneuvering motion simulation [J]. Ship Science and Technology, 2022, 44(14): 40-43.
[19] Wang Man-ning, Zhou Yu, Wang Meng-ying, et al. Influence of computational domain on flow characteristics of restricted jet flow in a pipe [J]. Building Thermal Energy, Ventilation, and Air Conditioning, 2018, 37(7): 33-36.
[20] Liu Yingzhong, Zhang Huaixin, Li Yile, et al. Ship Performance Calculation and RANS Equations in the 21st Century [J]. Ship Mechanics, 2001, 5(5): 66-84.
[21] LIU Y, LIU B, LEI J, et al. Numerical simulation of the hydrodynamics within octagonal tanks in recirculating aquaculture systems[J]. Chinese Journal of Oceanology and Limnology, 2017, 35:912-920.
[22] Gao Rui, Huang Wenchao, Zhang Bin. Study on the flow characteristics of particles in the drainage pipes of aquaculture vessels [J]. Modern Fisheries, 2021, 48(4): 61-69.
[23] Sun Di, Liu Fei. Optimization of wastewater discharge performance and bottom slope of aquaculture tanks based on CFD-DEM [J]. Journal of Fisheries Sciences of China, 2019, 43(4): 946-957.
[24] Zhang Chunjin, Sun Xihuan, Li Yongye, et al. Numerical simulation and verification of hydraulic characteristics of internal flow field in spiral flow inducer [J]. Transactions of the Chinese Society of Agricultural Engineering, 2018, 34(1): 53-62.
[25] Chen Min. Research on a method for predicting the hydrodynamic performance of stern propellers based on a fully structured grid [D]. Hubei: Huazhong University of Science and Technology, 2014.
[26] Gong Xiaodong, Yang Shujin, Liu Zuoshi. Simulation and structural optimization of the internal flow field of a Fluent centrifugal blood pump [J]. Chinese Journal of Medical Physics, 2022, 39(7): 913-918.
[27] Liu Changmeng, Gao Ye. Numerical simulation of airflow field on ski-jump deck [J]. Journal of Huazhong University of Science and Technology (Natural Science Edition), 2012, 40(10): 68-71.
[28] Wang Yan. Research on the dynamic analysis method of large centrifugal compressor impellers [D]. Liaoning: Dalian University of Technology, 2009.
[29] Xiang Honggui, Zhu Renzhuan, Miao Guoping, et al. Water flow and impact of waves on the deck of high-speed ships [J]. Research and Progress in Hydrodynamics A, 2010, 25(3): 277-284.
[30] Chen Shuling, Yang Songlin. Application of Fluent Software in Numerical Calculations for Surface Vessels [J]. Ship Science and Technology, 2012, 34(11): 37-41, 63.